Table S1 Lattice parameters and BET surface area of CP and FSP made $Ce_{1-x}Zr_xO_2$ catalysts.

CP-made $Ce_{1-x}Zr_xO_2$			FSP-made $Ce_{1-x}Zr_xO_2$		
x	LP[a] (Å)	BET (m^2/g)	x	LP[a] (Å)	BET (m^2/g)
0	5.41	NM[b]	0	5.41	NM[b]
0.20	5.36	103	0.20	5.35	103
0.46	5.26	74	0.45	5.27	96
0.74	5.17	50	0.70	5.18	99

[a] Lattice parameter

[b] Not measured

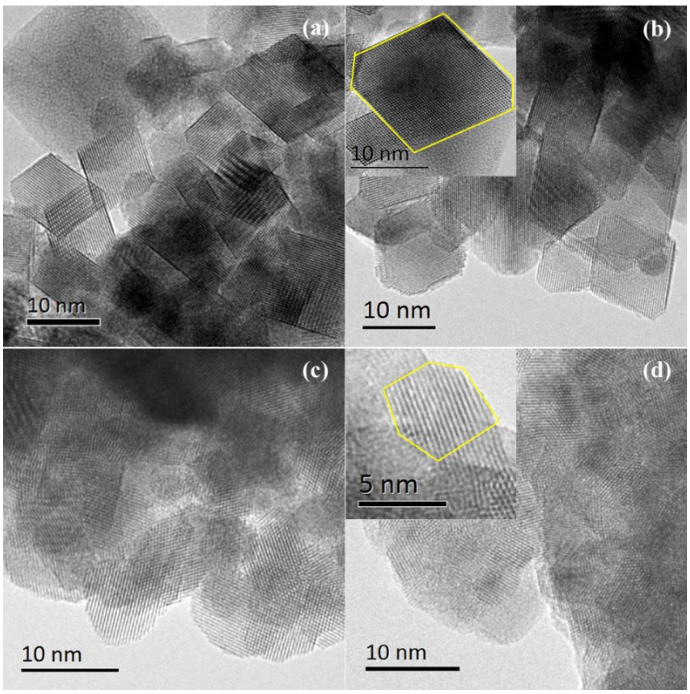

Figure S1 HRTEM images of (a) FSP-$Ce_{0.5}Zr_{0.5}O_2$; (b) FSP-$Ce_{0.25}Zr_{0.75}O_2$; (c) CP-$Ce_{0.5}Zr_{0.5}O_2$ and (d) CP-$Ce_{0.25}Zr_{0.75}O_2$, the insets show clearly particle shapes. Regular truncated octahedral particles with {111} and {100} as major facets are formed in FSP-made samples, while CP-made ones show irregular polygon geometries which resemble spherical particles in HRTEM images. FSP-made regular truncated octahedral particles are intermediates of the agglomeration after a high temperature calcination process, while CP-made irregular polygons or spherical particles are the final products.

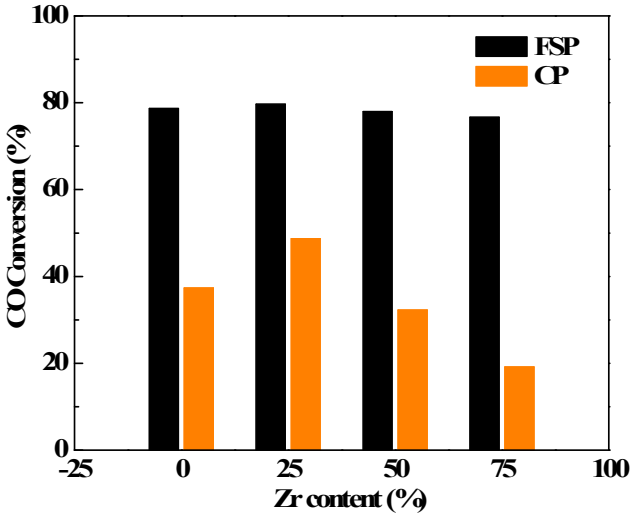

Figure S2 Catalytic performance of Ce-Zr oxide solid solutions made by FSP and CP methods in CO oxidation at 300 ºC and 0.1MPa in 1.66%CO/3.46%O_2/He balance atmosphere, space velocity is 12000ml/g·h. The CO conversion of FSP-$Ce_{1-x}Zr_xO_2$ almost stays at the same level for different Zr content, while they obviously exhibit a volcano type trend with the Zr content over CP-$Ce_{1-x}Zr_xO_2$.

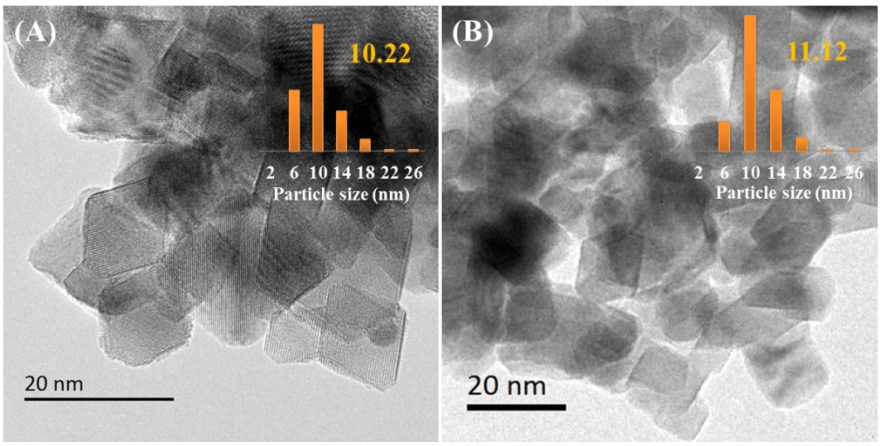

Figure S3 TEM images and particle size distribution of FSP-$Ce_{0.25}Zr_{0.75}O_2$ sample before (A) and after (B) thermal treatment at 800 ºC for 30h; the inset bar diagrams show the particle size distribution; the average particle sizes of fresh and calcined samples are 10.22 and 11.12 nm, respectively.

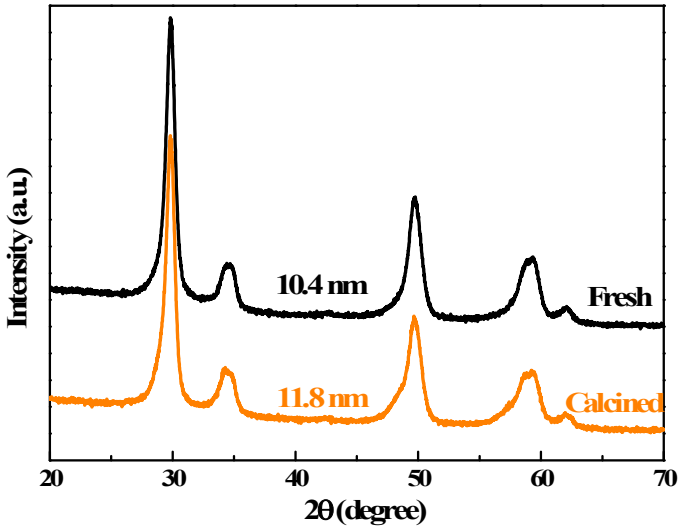

Figure S4 XRD patterns of fresh and calcined (800 ºC for 30h) FSP-$Ce_{0.25}Zr_{0.75}O_2$ samples and their crystal sizes calculated by Scherrerś equation.

Table S2 F2g peak position and shifts of fresh and calcined Ce-Zr oxide solid solutions with different Zr content

	Zr content%		
F2g peak position (cm^{-1})	25	50	75
CP-fresh	471.2	472.0	475.2
CP-calcined	474.4	473.3	458.2
Blue Shift (cm^{-1})	3.2	1.3	-17.0
FSP-fresh	465.8	466.1	461.7
FSP-calcined	471.5	473.1	470.0
Blue Shift (cm^{-1})	5.7	7.0	8.3

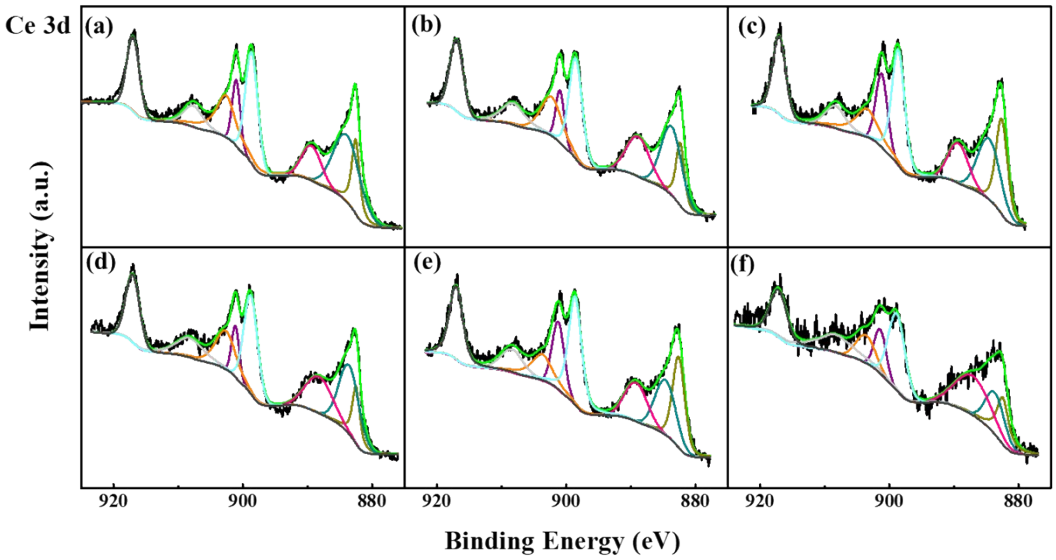

Figure S5. XPS spectra in Ce 3d of FSP (a, b and c) and CP (d, e and f) made $Ce_{1-x}Zr_xO_2$, where (a, d) x=0.25; (b, e) x=0.5; (c, f) x=0.75.

Table S3 Binding energies (eV) of Ce 3d and Ce^{3+}/Ce surface atomic ratios of tested samples

Samples	Ce 3d								Ce^{3+}/Ce
	V(Ce^{4+})	V'(Ce^{3+})	V'' (Ce^{4+})	V''' (Ce^{4+})	U(Ce^{4+})	U' (Ce^{3+})	U'' (Ce^{4+})	U''' (Ce^{4+})	
Au/FSP-$Ce_{0.75}Zr_{0.25}$	882.5(10%)	883.9(22%)	889.3(8%)	898.6(18%)	901.0(7%)	902.6(15%)	907.6(6%)	917.0(15%)	0.37
Au/FSP-$Ce_{0.5}Zr_{0.5}$	882.3(9%)	883.7(19%)	888.8(12%)	898.5(19%)	900.9(6%)	902.2(13%)	908.2(8%)	916.9(13%)	0.32
Au/FSP-$Ce_{0.25}Zr_{0.75}$	882.6(15%)	884.5(16%)	889.3(9%)	898.6(19%)	901.2(10%)	903.4(11%)	908.3(6%)	917.0(13%)	0.27
Au/CP-$Ce_{0.75}Zr_{0.25}$	882.5(9%)	883.6(19%)	888.3(13%)	898.8(19%)	901.1(6%)	902.7(13%)	908.2(9%)	917.0(13%)	0.32
Au/CP-$Ce_{0.5}Zr_{0.5}$	882.6(15%)	884.6(14%)	889.2(10%)	898.6(21%)	901.2(10%)	903.7(9%)	908.4(7%)	917.0(14%)	0.23
Au/CP-$Ce_{0.25}Zr_{0.75}$	882.4(11%)	883.6(11%)	887.1(19%)	898.8(19%)	901.4(7%)	903.6(7%)	908.2(13%)	917.1(12%)	0.19
FSP-$Ce_{0.25}Zr_{0.75}$	882.3(12%)	884.5(14%)	889.0(13%)	898.4(13%)	900.7(11%)	903.1(11%)	908.3(9%)	917.2(17%)	0.24
CP-$Ce_{0.25}Zr_{0.75}$	882.6(20%)	884.2(14%)	888.8(9%)	898.3(14%)	901.1(18%)	904.2(2%)	907.5(6%)	916.8(17%)	0.17

Table S4 F2g peak position and shifts of fresh and Au deposited Ce-Zr oxide solid solutions with different Zr content

	Zr content%		
F2g peak position (cm^{-1})	25	50	75
CP-fresh	471.2	472.0	475.2
Au/CP	460.1	463.8	462.6
Red Shift (cm^{-1})	11.1	8.2	12.6
FSP-fresh	465.8	466.1	461.7
Au/FSP	451.7	453.5	432.1
Red Shift (cm-1)	14.1	12.6	29.6

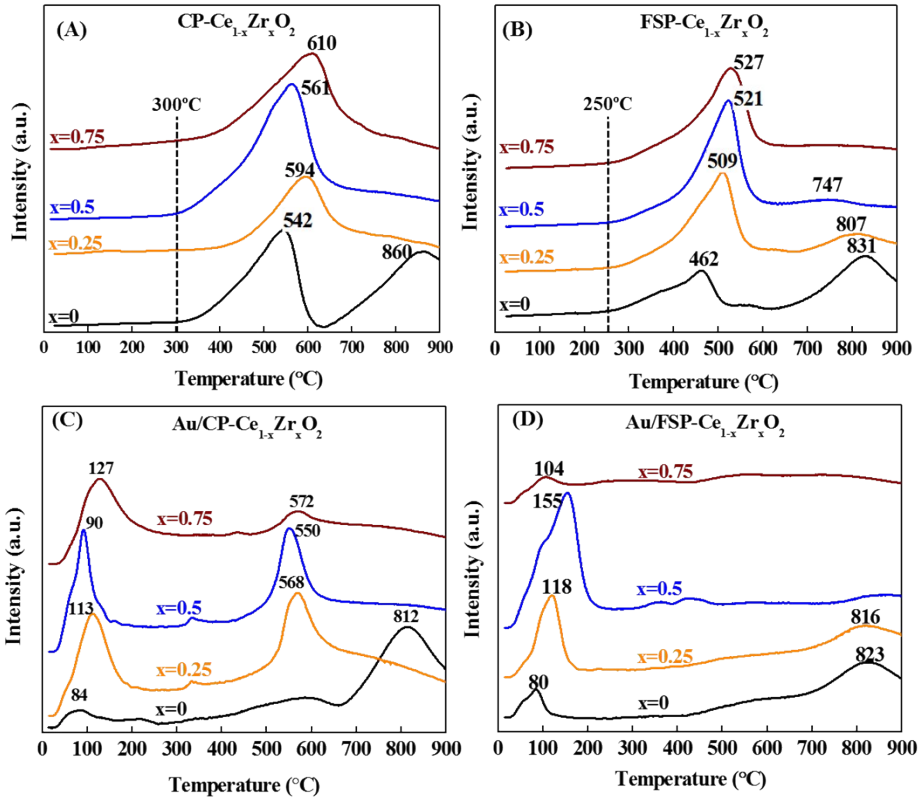

Figure S6. TPR results of Ce-Zr oxide solid solutions before and after Au deposition.